Dynamics of Spontaneous Spreading on Heterogeneous Surfaces in a Partial Wetting Regime

S. Semal, M. Voué, M. J. de Ruijter, J. Dehuit, and J. De Coninck*

Centre de Recherche en Modélisation Moléculaire, Université de Mons-Hainaut, 20, Place du Parc, B-7000 Mons, Belgium

Received: December 4, 1998; In Final Form: March 15, 1999

We show how the surface coverage of partially *n*-octadecyltrichlorosilane (OTS) grafted silicon wafer can be estimated from dynamical wetting measurements. By use of the molecular kinetic theory of wetting, values of the effective jump frequency are determined from the relaxation of the contact angle of branched alkane droplets on such heterogeneous substrates. These jump frequencies are correlated to the OTS thickness measured by ellipsometry. The surface composition can then be calculated, indicating the strong influence of the transition from the expanded to the condensed liquid phase on the wetting properties of the substrate.

1. Introduction

When a liquid drop is placed in contact with a substrate, capillary forces drive the interface spontaneously toward equilibrium. As the drop spreads, the contact angle θ relaxes from its initial maximum of 180° at the moment of contact to its equilibrium angle $\theta_0 > 0°$ in the case of partial wetting or 0° if the liquid spreads completely.

The dynamics of spontaneous spreading are usually described at the macroscopic level by an energy balance between the capillary driving force and the hydrodynamic resistance to spreading.[1−3] The experimental results more or less fit master curves showing relationships between the radius of the base and time or between contact angle and time. The macroscopic parameters of these master curves are the surface tension and viscosity of the liquid, the volume of the drop, and some cutoff or slip length.

It is also possible to describe the spontaneous spreading of a liquid drop in terms of microscopic quantities, specifically the jump frequency K_W^0 and length λ of the liquid molecular displacements in the vicinity of the substrate, near the wetting line. Indeed the molecular kinetic theory of wetting,[4] due to Blake and Haynes, allows one to link these microscopic quantities, K_W^0 and λ, with the macroscopic dynamical behavior of the contact angle within the partial wetting regime.

All these theories deal with ideal flat and chemically pure substrates. However, these conditions are particularly difficult to obtain and to maintain from the experimental point of view. Both roughness and chemical heterogeneities will drastically change the dynamics of spreading.[5−8] Hence, there is a need to control the nature, the distribution, and the size of the heterogeneities and to understand the dynamic behavior of the contact angle on heterogeneous substrates.

Conversely to what happens in the experiments, the substrates investigated in computer simulations can be at the same time heterogeneous and perfectly controlled at the microscopic level. A few attempts have been made to describe the dynamics of wetting of heterogeneous substrates [refs 9−11 and references therein]. By use of Monte Carlo simulation techniques in particular, the influence of the geometry of a rough surface on the wall tension has also been studied.

More recently, molecular dynamics simulations were used to study the dynamics of relaxation of the contact angle of sessile drops in the partial wetting regime.[12] The investigated substrates were ideally flat but chemically heterogeneous. In that study, the size and the distribution of the heterogeneities were perfectly controlled. The validity of Cassies's law[13] was demonstrated at the microscopic scale. Indeed, the authors found that the equilibrium contact angle θ_0^{AB} of sessile drops on a mixed substrate AB is a function of the contact angles measured on the two pure substrates A and B, θ_0^A and θ_0^B, respectively:

$$\cos \theta_0^{AB} = c \cos \theta_0^{A} + (1 - c) \cos \theta_0^{B} \qquad (1)$$

where c and $(1 - c)$ denote the relative surface concentration of species A and B, respectively. Moreover, from the time variations of the positions of the considered atoms, it was possible to observe the relaxation process itself of the sessile drop on the mixed substrate as a function of the concentration of the heterogeneities. As already successfully done in the case of pure substrates,[4,14,15] it was found that the molecular kinetic theory[4] was appropriate for determining the effective jump frequency of the liquid molecules on the heterogeneous substrate. A simple theory was proposed to describe the variations of the frequency as a function of c.

The present study addresses the same problem from the experimental point of view. We report here the results of experiments devoted to the dynamics of spontaneous spreading of droplets on chemically heterogeneous substrates. The paper is organized as follows. Section 2 is devoted to the presentation of the experimental setup and materials. The results and their analysis are presented in section 3. Concluding remarks are given in section 4.

2. Experimental Setup and Materials

2.1. Chemical Grafting. Self-assembled organic monolayers (SAM) on solid substrates provide an interesting approach to design-tailored surfaces with controlled physical and chemical properties.[15] SAM's of *n*-alkyltrichlorosilanes on silica surfaces attract strong interest in several fields such as physical chemistry, material science, and biology and have been used in a number

10.1021/jp984609m CCC: $18.00
Published on Web 05/22/1999

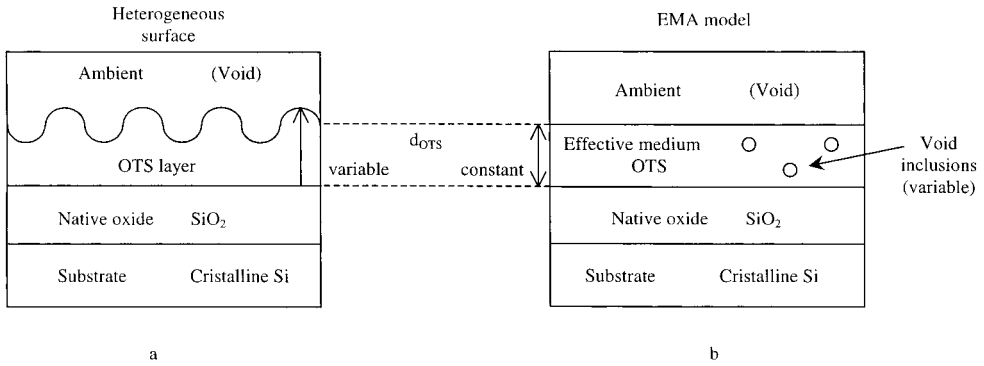

Figure 1. Surface heterogeneities and optical model of a partially OTS grafted monolayer on native oxide layer covering a silicon wafer: (a) heterogeneous surface, where the thickness d_{OTS} of the compact monolayer varies from point to point; (b) EMA, where the optical properties of void and OTS are mixed together at variable concentrations (the thickness d_{OTS} is constant) to describe the optical properties of the heterogeneous layer.

of applications, including wetting,[17] sensors,[18] molecular electronics,[19] and protein adsorption.[20]

SAM's are constructed by using amphiphilic molecules whose small functional headgroup shows an affinity for the substrate, combined with an aliphatic tail. Silicon wafer is the most commonly used substrate. We used *n*-octadecyltrichlorosilane (OTS, Sigma, 99%) to cover the wafers with a monolayer. The self-assembling process requires two steps.[21] First, the molecules (or hydrolyzed molecules) are adsorbed onto the surface and organize themselves. Then, provided that the substrates exhibit the right chemical sites, the organized film is covalently grafted to the surface.

OTS was packaged in individual small bottles under dry N_2 flow to avoid contact with ambient air, which could cause self-polymerization, which manifests itself as flakes in the solution or as a thin haze at the liquid surface and is easily detected.

Monocrystalline (100) silicon wafers (Siltronix, France), covered by their native oxide layer (about 20 Å), were used as substrates. These wafers exhibit one polished side, being atomically flat over 200 × 200 Å^2 areas separated by a few anstrom steps.

The first step, before the grafting procedure, is the cleaning of the surfaces. The procedure described in ref 22 has been used. The substrates were then immersed in a reaction bath ($T = 12 \pm 1$ °C, RH $= 47 \pm 3\%$) of freshly prepared millimolar solution of OTS in *n*-hexadecane (Sigma, 99%) and carbon tetrachloride (Sigma, 99%) in a 7:3 volumetric ratio. The solvents were previously dried using a 4 Å molecular sieve. The immersion time in the reaction bath (henceforth referred to as the "reaction time") controls the coverage of the solid by OTS. We considered reaction times from 10 s to 6 h. After the latter reaction time, no more modification of the substrate was detected by means of contact angle, AFM, and spectroscopic ellipsometry measurements. To remove all excess chemicals after the reaction, the samples were sonicated in two successive chloroform baths for 3 min. The chemical grafting of silane molecules to the silica surface "freezes" their conformation.[21]

Several recent studies[21,23,24] were devoted to the molecular organization of these SAM's. Let us briefly review their main results. The surfaces exhibit two types of areas covered with OTS: dense condensed assembly of molecules and disordered molecules that have not self-assembled to form condensed domains, referred to as LC* phase (liquid condensed) and LE* phase (liquid expanded), respectively, by analogy to the Langmuir films. Monte Carlo simulations of the growing process of the dense condensed islands using a two-dimensional diffusion-limited aggregation support this model.[23] AFM measurements show that the coverage consists of domains of different sizes and shapes, including fingering patterns.[21] The latter study shows that the complete coverage corresponds to a uniform LC* phase.

2.2. Spectroscopic Ellipsometry. To characterize the quality of the substrate grafting, spectroscopic ellipsometry has been used. This experimental technique measures the change in the polarization state of the light when the incident beam is reflected on an interface. More precisely, if r_p and r_s denotes the complex overall reflectance of the p (parallel) and s (perpendicular) components of the incident wave at the surface of an optical multilayer structure, the complex ratio

$$\rho = \frac{r_p}{r_s} = \tan \Psi \, e^{-\Delta} \qquad (2)$$

defines the ellipsometric angles Ψ and Δ. ρ is a complex nonlinear function of the refractive indexes of the materials, their thicknesses, the wavelength, and the incidence angle of the beam.[25,26] Except in the case of an ideally flat bare substrate, this equation cannot be analytically inverted and nonlinear optimization methods are used to extract the thickness of the layer from the ellipsometric data over the whole range of investigated wavelengths.

From the experimental point of view, roughness is clearly a relative quantity. If the techniques are optical, then it depends on the ratio of the length scale of the irregularities to the wavelength of the incident light. When the influence of microscopic heterogeneities has to be considered, i.e., when the mean height and correlation length of the surface heterogeneities are both much less than the wavelength of the light, the beam interacts with the surface as a whole rather than with each individual irregularity.[26]

Two models can be used to characterize rough samples by ellipsometry.[25] In the first one (Figure 1a), the rough layer is described as a compact one-component layer of variable thickness, while in the second one (Figure 1b), the effective medium approximation (EMA) is used.

An interesting, although not recent, review of the investigation of effective medium models of microscopic surface roughness by spectroscopic ellipsometry has been published by Aspnes and co-workers.[27] Under these assumptions of microscopic surface roughness, multiple scattering depolarization is not significant and the contribution of the field-induced polarization of the rough surface to the far-field radiation pattern measured experimentally can be approximated by one or more layers of a polarizable effective medium that is sandwiched between an ideally flat substrate and a perfect ambient medium. The qualitative similarity and quantitative differences of the various

effective medium approximations are discussed in ref 27. Several simple models such as the Lorentz−Lorentz (LL), Maxwell−Garnett (MG), and Bruggeman effective medium approximation (EMA) models have been proposed to describe the optical properties of such effective mediums.[28,29] All of them represent a heterogeneous dielectric mixture by a single parameter. Therefore, they are natural first approximations for describing the behavior of a rough surface layer. In particular, the EMA has been widely used to take into account the effects of the surface heterogeneities.

Let us recall the basis of this approach. For a *n*-component mixture, the complex dielectric function ϵ_e of the effective medium, related to its refractive index N_e by $\epsilon_e = N_e^2$, is given by

$$\frac{\epsilon_e - \epsilon_h}{\epsilon_e + 2\epsilon_h} = \sum_{i=1}^{n} f_i \frac{\epsilon_i - \epsilon_h}{\epsilon_i + 2\epsilon_h} \tag{3}$$

where ϵ_i and ϵ_h denote the complex dielectric function of the *i*th component and of the host medium h, respectively, and f_i denotes the volume fraction of the *i*th component in the total mixture. The main difference between the different models lies in the choice of the "host" medium. But, irrespective to this choice, the underlying assumptions of the mixing rule (eq 3) are based on spherical inclusion geometry and dipole interactions. As highlighted by Aspnes et al.,[27] neither assumption is rigorously satisfied by a rough layer, but in the absence of resonances the modifications of the depolarization factor from the spherical value of $^1/_3$ are not generally significant, and the dipole interaction is a standard first approximation. Bruggeman[29] considered the host as being the effective medium itself, which yields, for a two-component mixture, the following equation:

$$f\frac{\epsilon_1 - \epsilon_e}{\epsilon_1 + 2\epsilon_e} + (1 - f)\frac{\epsilon_2 - \epsilon_e}{\epsilon_2 + 2\epsilon_e} = 0 \tag{4}$$

allowing the complex dielectric function of the effective medium ϵ_e to be directly calculated from the dielectric function of its constituents ϵ_1 and ϵ_2. Therefore, the grafted OTS layer (Figure 1a) may be described by the following simple model: an effective layer whose thickness is equal to the thickness of the grafted OTS molecule and whose constituents are the OTS itself at volume fraction *f* and void inclusions (Figure 1b). It should be noted that eq 4 is symmetrical with respect to each constituent and that therefore no special role is devoted either to OTS or to the void inclusions, allowing us to use the model over the entire range of volume fractions ($0 < f < 1$).

As we are dealing with very thin layers (the thickness of the OTS molecule is about 22.0 Å, as shown below), there is a lack of optical contrast between the native oxide layer present at the surface of the wafer and the OTS itself. For this reason, the optical properties of the OTS will be considered equal to the ones of the SiO_2 layer, irrespective to its nature, either LE* or LC* phase. A similar approach to consider identical optical properties has been used for hexamethyldisilazane and hexadecyltrichlorosilane grafted layer on top of silicon wafers.[30]

The ellipsometric measurements were carried out with a SOPRA GESP5 rotating polarizer instrument with an intensified photodiode array (IPDA) detector allowing the acquisition of the ellipsometric data at 512 energies in the 1.5−4.5 eV range. The polarizer rotates at 9 Hz, and the analyzer angle was set to 20°. The spectroscopic ellipsometer operates at 75° of incidence, close to the Brewster's angle for silicon. With the use of microspots, the diameter of the beam originating from a xenon lamp (Hamamatzu Inc.) is reduced from 4 mm (parallel beam configuration) to 80 μm.

2.3. Contact Angle Measurements. The liquid we used to measure the wetting characteristics of the substrates was squalane (2,6,10,15,19,23-hexamethyltetracosane, $C_{30}H_{62}$), a nonpolar branched hydrocarbon (Sigma, 99%). Squalane has a surface tension γ_{LV} of 31.1 mN/m and a viscosity of 35.0 mPa s at a temperature of 21 °C.[15] The substrate was placed on a movable stage in front of a microscope, and a squalane droplet (volume of ~6 mm^3) was deposited with a syringe. Within a few seconds the droplet spread and reached its static contact angle. The relaxation of the liquid was slow enough to allow us to follow in detail the time behavior of the contact angle. The microscope was connected to a black-and-white CCD camera, and the images (768 × 576 pixels, 256 gray levels) of the droplet were captured on a video recorder (VCR) at the speed of 50 images per second. Pictures were then selected from the videotape and grabbed by a computer (Data Translation DT3551 frame grabber) for further analysis. During all the experiments reported in this article, the room temperature was 21 ± 1 °C. After the localization of the edge of the liquid/gas interface, the shape of sessile drops in the presence of gravity is described by the Laplace equation[31]

$$\Delta P = \gamma\left(\frac{1}{R_1} + \frac{1}{R_2}\right) \tag{5}$$

which relates the surface tension of the liquid to the pressure difference across the liquid/gas interface, R_1 and R_2 being the two principle radii of curvature of the curved surface. The best Laplace curve is fitted through the experimental profile (about 1500 experimental points)[14,32] by combination of the downhill simplex minimization method with a Runge−Kutta algorithm.[33] From the fit, the contact angle is easily determined.

3. Results

3.1. Spectroscopic Ellipsometry. Before each grafting experiment, the thickness of the native oxide layer was measured and was considered as a reference thickness. As already mentioned, after a reaction time of 6 h, no more modification of the substrate is detected by means of both contact angle and ellipsometric measurements; the substrate is totally grafted. The measured thickness of the complete OTS layer, assuming that the refractive index of the OTS layer is not too different from the SiO_2 one, is 22.1 Å. This result, consistent with values found in the literature,[16,17,21] will constitute the upper bound of our concentration scale.

In Figure 2, we show the relation between the relative thickness of the grafted layer h/h_{max}, where h_{max} is the thickness of the layer measured on the totally grafted substrate, and the corresponding OTS volume fraction in the same grafted layer, as determined from the EMA, knowing the maximum thickness of the SAM (h_{max} = 22.1 Å) and the optical properties of its constituents. Although obviously nonlinear, this relation is monotonic and clearly shows that both measured quantities, i.e., either the OTS volume fraction or the averaged relative height, may be used to characterize unambiguously the coverage of the samples.

As roughness is typically dependent on the considered length scale, ellipsometric data were initially measured without microspot on a loose square grid of 25 measurements (lateral resolution of about 2 mm; grid spacing of 5 mm). To observe the effect of the grid size on ellipsometric measurements,

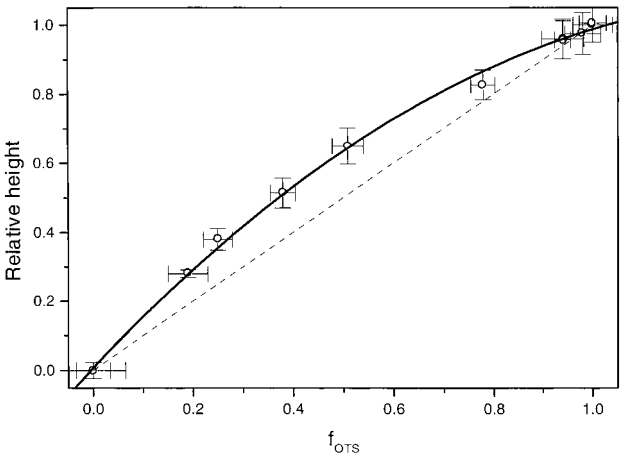

Figure 2. Characterization of the grafting using spectroscopic ellipsometry. The relative height h/h_{max} (h_{max} = 22.1 Å) is a nonlinear function of the OTS thickness fraction f_{OTS}. The error bars are the standard deviations of the relative height (or thickness fractions) determined on 121 experimental measurements. The plain curve acts only as a guide for the eye.

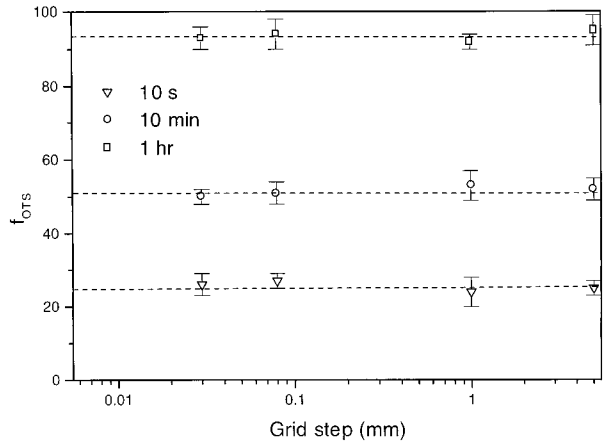

Figure 3. Influence of the measurement grid step on the OTS thickness fraction f_{OTS} for reaction times of 1 s, 10 min, and 1 h, respectively. The error bars are the standard deviations of the thickness fractions determined on 121 experimental measurements. f_{OTS} appears to be independent of the length scale over the whole range of coverage.

subsequent mappings were done with the 80 μm beam on grids of 11 × 11 points of 1 mm, 300 and 80 μm steps in both *X* and *Y* directions. These OTS volume fractions were measured on substrates after 10 s, 10 min, and 30 min reaction times and are represented in Figure 3 as a function of the size of the 11 × 11 grids of analysis. As indicated by the low values of the error bars, the surface coverage is homogeneous and the OTS volume fraction is independent of the length scale over the range at which it was measured. The statistical error associated with each value of f_{OTS} and originating from the numerical analysis of the ellipsometric data is less than 5×10^{-4}, showing that the main error source is the distribution of the f_{OTS} values, from one site to the other.

This OTS volume fraction in the monolayer will be used throughout the rest of this article to characterize the grafting of the substrates. Its dependence on the grafting reaction time is presented in Figure 4. Within the error bars, 80% coverage is reached after 30 min, and 3 h are necessary to obtain an almost complete coverage.

3.2. Wetting Dynamics. *3.2.1. Experimental Results.* To determine the effect of heterogeneities on the dynamics of spreading, we have measured the dynamic advancing contact angle of droplets of squalane spreading spontaneously on the partially grafted surfaces.

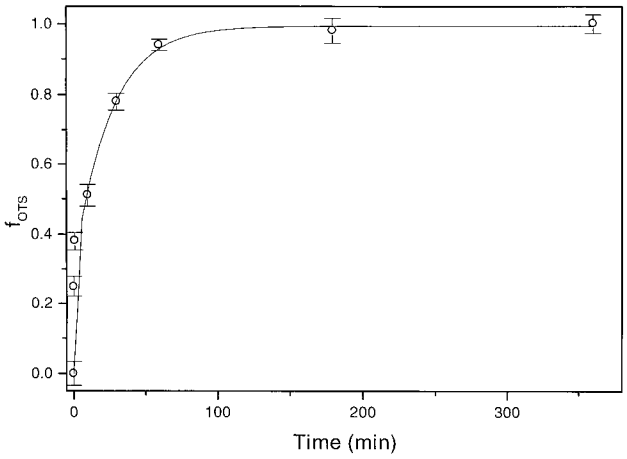

Figure 4. Time variation of OTS volume fraction. The plain curve acts only as a guide for the eye.

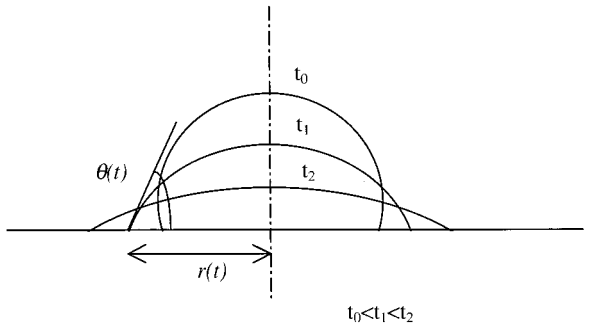

Figure 5. Spreading of a sessile drop of a liquid. *r(t)* and $\theta(t)$ are, respectively, the base radius and the contact angle of the drop.

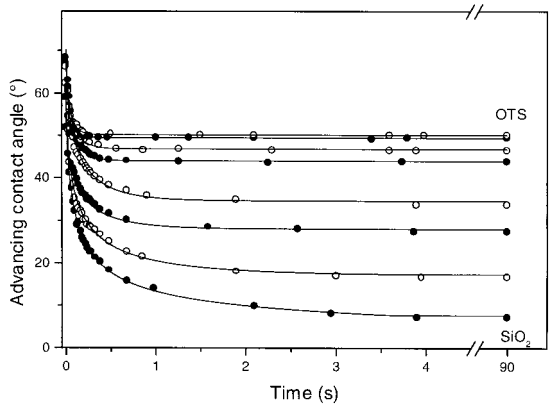

Figure 6. Dynamic contact angles vs time for spontaneous spreading of squalane droplets on partially grafted substrates. The dynamic advancing contact angle is represented vs the relaxation time for substrates prepared with different reaction times. Reaction times were (from bottom to top) 0 s, 10 s, 1 min, 10 min, 30 min, 1 h, 3 h, and 6 h. The lowest curve corresponds to the bare silicon wafer. Solid lines correspond to theoretical fits using the molecular kinetic theory (eq 6).

The initial shape of a liquid drop placed on the top of a substrate will be different from the equilibrium case. To minimize the free energy of the system, the drop will transform itself as a function of the time. At constant volume, this dynamic behavior is characterized by the contact angle $\theta(t)$ (Figure 5).

The results for spontaneous spreading of squalane drops on the different substrates are shown in Figure 6, where the dynamic contact angle has been plotted versus time.

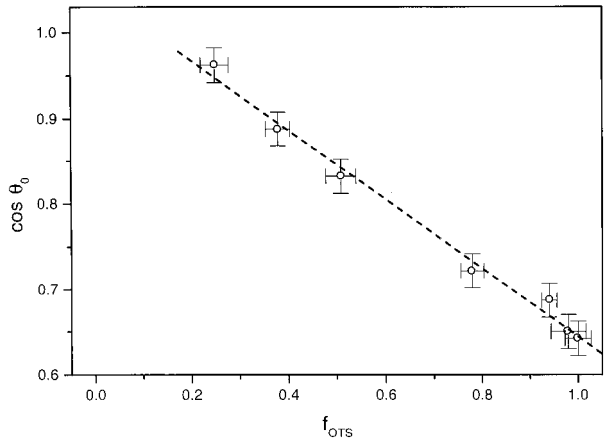

Figure 7. Cosine of the equilibrium contact angle of squalane droplets vs the OTS volume fraction. cos θ_{eq} varies linearly with f_{OTS} between 0.2 and 1.0.

The static contact angle θ_0 is reached after times from a few tenths of seconds, for completely grafted substrates, to a few seconds, for bare ones. The cosine of the static contact angle varies linearly for the OTS volume fraction between 0.3 and 1.0 (Figure 7). This result is in agreement with a Cassie-like law.[13] Since the squalane droplet wets the bare silica surface and since the "wetting/nonwetting" transition is not precisely localized, the data corresponding to the pure silica surface have not been taken into account, in a view of not inducing a bias in the determination of the transition.

3.2.2. Discussion. Since we want to relate the modifications of the wettability of the substrate due to the grafting to parameters controlling the displacement of the liquid molecules at the interface, we choose the molecular kinetic theory[4] to interpret the experimental data. This theory relates the dynamic angle θ and the velocity v of the wetting line:

$$v = \frac{dr}{dt} = 2K_W^{\circ}\lambda \sinh\left[\frac{(\cos\theta_0 - \cos\theta)\gamma_{LV}}{2k_B nT}\right] \qquad (6)$$

where K_W^0 is the equilibrium jump frequency of the liquid molecules at the wetting line (when the wetting line is at equilibrium), λ is the distance between adsorption sites, k_B the Boltzmann's constant, n the surface density of sites on the surface, and T the absolute temperature.

For small drops, gravity can be neglected and the shape of the spreading drop will approximate a spherical cap. The geometry of a spherical cap is then characterized by the following relationship:

$$r = \left(\frac{3V}{\pi}\frac{\sin^3\theta}{2 - 3\cos\theta + \cos^3\theta}\right)^{1/3} \qquad (7)$$

where V is the drop volume.[14,31]

Taking advantage of the very low volatility of the squalane at 21 °C and of the short time scales of the contact angle relaxation process (Figure 6), the droplet volume can be considered constant, yielding the following equation for the time variation of the base radius:

$$\frac{dr}{dt} = -\frac{d\theta}{dt}\left(\frac{3V}{\pi}\right)^{1/3}\left(\frac{(1-\cos\theta)^2}{2 - 3\cos\theta + \cos^3\theta}\right)^{4/3} \qquad (8)$$

Equations 6 and 8 are a linked pair of partial differential equations. The static contact angles values are those obtained experimentally. Thus, these equations may be solved numerically

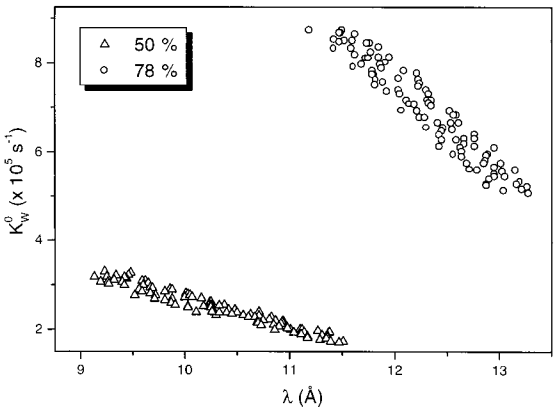

Figure 8. Distributions of the K_W^0 and λ values as calculated using the bootstrap method for the 50% and 78% grafted substrates. The mean values of the distributions correspond to the time relaxation of the contact angle of a squalane droplet spreading on a 10 min partially OTS grafted silicon wafer. The correlation between the K_W^0 values and the λ values is due to eq 6.

with two adjustable parameters: the prefactor $K_W^0\lambda$ and $\gamma_{LV}/(2k_BnT)$. In first approximation n and λ are related by $n = \lambda^{-2}$.[4] This procedure was used to fit the experimental data in Figure 6 and to determine the K_W^0 and λ values as a function of the substrate coverage. As can be seen, the fits are of good quality.

To estimate the associated errors, we have applied the bootstrap method.[33] We use the original experimental data as the basis of a Monte Carlo simulation. From this original set, 37% (i.e., 1/e) of the randomly chosen points are replaced by duplicates from the original data according to

$$\theta_{duplicate} = \theta_{original} + \xi\Delta\theta_{max} \qquad (9)$$

where $\Delta\theta_{max}$ is the maximum allowed variation fixed to 1° (i.e., corresponding to the maximum experimental deviation) and ξ a random number normally distributed around a zero mean with a unit variance. Using this procedure, we replace the original data set by a new one for which the corresponding parameters K_W^0 and λ can again be calculated. Typically, 100 successive simulations were considered and the distribution of values for each parameter statistically was analyzed. Figure 8 shows the results obtained for a 51% grafted surface (10 min). Analogous results are obtained for the other surfaces. The correlation between the K_W^0 and λ shown in Figure 8 results from the applicability of the linearized form of eq 6

$$\frac{dr}{dt} = \frac{K_W^{\circ}\lambda^3}{k_BT}(\cos\theta_0 - \cos\theta) \qquad (10)$$

since the order of magnitude of the sinh argument is significantly less than unity in these experiments.

Table 1 gives the values of the two parameters K_W^0 and λ obtained after the complete fitting procedure. The mean values and standard deviation are calculated from the distribution obtained after 100 simulations. λ is more or less constant (about 11.3 Å) for the whole range of coverage while K_W^0 is about $2 \times 10^5\ s^{-1}$ for OTS volume fractions between 0% and 50% and increases strongly for volume fractions above 50% (Figure 9). For substrates characterized by these fractions, K_W^0 appears to be highly sensitive to the coverage. As long as the grafting is not complete, it will not reach its maximum value.

To interpret these results, we have to reconsider the growing process of an OTS grafted monolayer on silicon wafer according

TABLE 1: Jump Frequency K_W^0, Intersite Distance λ and Static Contact Angle θ_0, Determined from Molecular Kinetic Theory vs the OTS Volume Fraction f_{OTS} Determined from Ellipsometry ($m \pm$ sd, $n = 100$)[a]

f_{OTS}	λ (Å)	K_W^0(10^5 s^{-1})	θ_0 (deg)
0.0	10.3 ± 0.4	1.4 ± 0.8	0 ± 1.0
0.25 ± 0.03	12.0 ± 0.6	2.0 ± 0.5	16.7 ± 1.0
0.38 ± 0.02	11.2 ± 0.3	1.6 ± 0.7	27.9 ± 1.0
0.51 ± 0.03	10.3 ± 0.7	2.5 ± 0.8	34.6 ± 1.0
0.78 ± 0.04	12.3 ± 0.5	6.9 ± 1.8	43.9 ± 1.0
0.94 ± 0.03	11.4 ± 0.5	21.4 ± 3.2	46.9 ± 1.0
0.98 ± 0.04	11.8 ± 0.4	28.6 ± 2.2	49.6 ± 1.0
1.0 ± 0.03	10.7 ± 0.5	31.6 ± 2.7	50.2 ± 1.0

[a] The given values correspond to average quantities over 100 independent runs applying the bootstrap method. The error bars are the statistical standard deviations.

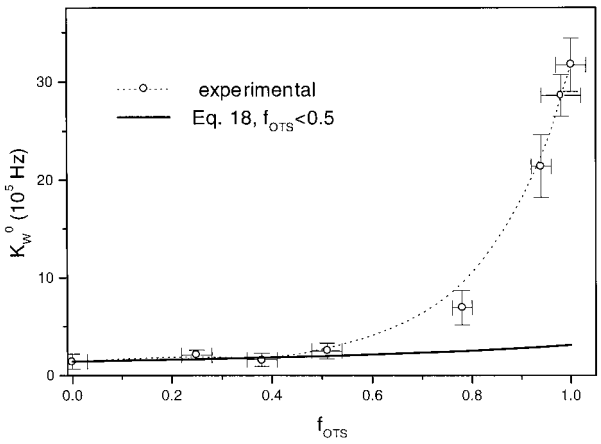

Figure 9. Jump frequency K_W^0 vs the OTS volume fraction f_{OTS}. K_W^0 remains constant at low coverage of the substrate and sharply increases when the transition between the expanded liquid phase (LE*) and the condensed liquid phase (LC*) occurs. The solid line corresponds to the linear approximation given by eq 16 for low values of f_{OTS}. The dotted line represents eq 14.

to the model proposed in ref 21 for grafting at 12 °C. First, the cleaned and therefore highly reactive bare SiO_2 surface is covered by a loose layer of adsorbed (not chemically anchored) molecules that are in an expanded liquid (LE*) phase. Although some islands of anchored molecules are sometimes observed during the first seconds of the reaction process, the coverage of the whole surface with molecules in the LE* phase is dominant. After this initiation stage, the anchoring takes place and the final monolayer is made up of molecules in a condensed liquid (LC*) phase. For completely grafted substrates, both AFM and ellipsometry observations show that the monolayer is homogeneous, exhibits a low roughness[21] and is 22.1 ± 0.8 Å thick (h_{LC*}). It is therefore interesting to interpret the wetting behavior of the investigated samples in terms of their surface composition.

To determine to which extent this composition will influence the time relaxation of the contact angle, let us consider the displacement of the three-phase line of a liquid on a heterogeneous substrate consisting of successive patches of different materials of respective width L_i, $i = 1, ..., N$. On each of these patches, the displacement of the considered liquid can be characterized by a friction coefficient ζ_i (Figure 10).

The total time t required for the contact line to move from A to B, following the path indicated in Figure 10, is given by

$$t = \sum_i t_i + \sum_i \tau_{i,i+1} \tag{11}$$

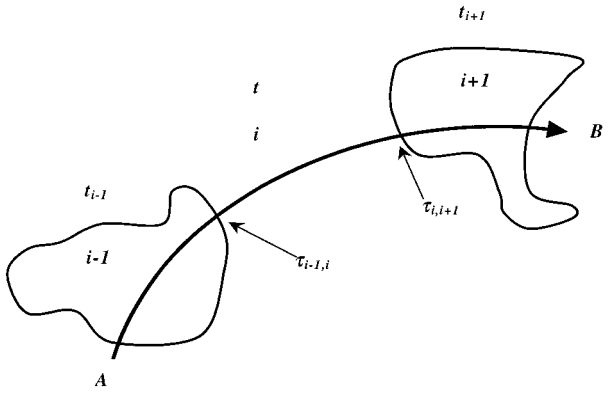

Figure 10. Model associated with a heterogeneous surface consisting of macroscopic patches of different materials of respective length L_i, $i = 1, ..., N$. On each of these, the displacement of the considered liquid is characterized by a friction coefficient ζ_i. t_i and $\tau_{i,i+1}$ are, respectively, the time spent on the ith patch and the time eventually required to move from the ith material to the $(i+1)$th one. v_i is the speed of the contact line on the ith patch.

where t_i and $\tau_{i,i+1}$ are, respectively, the time spent on the ith material and the time eventually required to move from the ith material to the $(i + 1)$th one. If the substrate is macroscopically heterogeneous or if the difference in wettability between the different materials is small, the second term in eq 11 or the individual $\tau_{i,i+1}$ contributions are negligible with respect to $\sum_i t_i$. Assuming a constant driving force F and the viscous nature of the friction, i.e., $F = \zeta_i v_i$, with v_i the speed of the contact line on the considered patches, the effective friction ζ_{eff} is given by

$$\zeta_{eff} = \sum_i \zeta_i c_i \tag{12}$$

where $c_i = L_i/(\sum_j L_j)$ is the surface fraction of the ith material. Since each of the friction coefficients can be expressed as the inverse of a jump frequency $K^0_{W,i}$,[31] we obtain an equation that relates the effective jump frequency $K^0_{W,eff}$ to the individual frequencies and the surface composition:

$$\frac{1}{K^0_{W,eff}} = \sum_i \frac{c_i}{K^0_{W,i}} \tag{13}$$

Within this derivation, it is implicitly assumed that λ is constant, in agreement with the experimental results. Considering now the growing process of an OTS monolayer, we obtain

$$\frac{1}{K_{eff}} = \frac{c_{SiO_2}}{K_{SiO_2}} + \frac{c_{LE*}}{K_{LE*}} + \frac{c_{LC*}}{K_{LC*}} \tag{14}$$

where the sub- and superscripts W and 0 have been omitted and where SiO_2, LE*, and LC* correspond to the bare silica, the expanded liquid, and the condensed liquid phases, respectively. Of course, for other types of these three phase lines, such as stick ones, we may expect other types of relationship.

Equation 14 is therefore a three-phase model that is fully compatible with the two-phase model (eq 4) used to compute f_{OTS} from the ellipsometric data because the optical properties of both the LE* and LC* phases are assumed to be not too different from the ones of the SiO_2 phase. Experimentally, these differences will not be measured as long as the thickness of the grafted layer remains low, i.e., as long as we are dealing with SAM's.

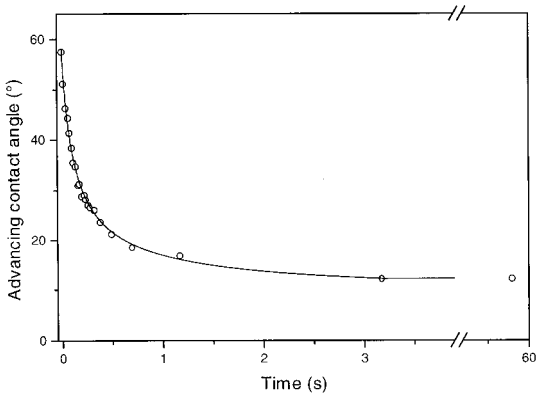

Figure 11. Time relaxation of a squalane droplet on a silicon wafer completely covered by OTS molecules in a LE* phase. The plain line corresponds to the fit using the molecular kinetic theory (eq 6). The best-fit values of K_{LE^*} and of λ_{LE^*} are 1.96×10^5 Hz and 9.2 Å, respectively.

The effective jump frequencies K_{eff} are measured for each of the partially grafted substrates (Figure 9). Those of the reference phases K_{SiO_2} and K_{LC^*} determined for the bare silica surface and for the completely grafted substrate are equal to 1.42×10^5 and 31.6×10^5 Hz. The determination of K_{LE^*} requires completely different experimental conditions, as explained below.

According to ref 22, the grafting at a temperature higher than 28 °C will lead to the formation of a monolayer made up only of molecules in a LE* phase. We have performed the grafting of this phase at 45 °C. AFM observations and ellipsometry measurements show that the LE* monolayer completely covers the substrate, is homogeneous, exhibits a low roughness,[21] and is 11.3 ± 0.9 Å thick (h_{LE^*}), yielding a thickness ratio $h^* = h_{LE^*}/h_{LC^*}$ equal to 0.51. As shown in Figure 11, the equilibrium contact angle of a squalane droplet on such a surface is equal to 12.4°. The corresponding jump frequency K_{LE^*} is 1.96×10^5 Hz, a value slightly higher than the one measured for the bare silica surface. λ_{LE^*} is equal to 9.2 Å.

Let us now consider separately the results obtained on the silicon wafers partially OTS grafted (Figure 12) for the early and late stages of the process.

In the early stage, the term c_{LC^*}/K_{LC^*} in eq 14 can be neglected because the condensed liquid phase is almost not present ($c_{LC^*} \ll 1$) at the surface and because the jump frequency K_{LC^*} is 1 order of magnitude higher than K_{SiO_2} and K_{LE^*}. Therefore, the effective jump frequency K_{eff} is given by

$$\frac{1}{K_{eff}} \cong \frac{c_{SiO_2}}{K_{SiO_2}} + \frac{c_{LE^*}}{K_{LE^*}} \tag{15}$$

The relative surface concentrations c_{SiO_2} and c_{LE^*} are not directly available from the spectroscopic ellipsometry measurements. Only the total OTS volume fraction f_{OTS} is available. For the short reaction times, $f_{LE^*} = f_{OTS}$. By use of simple geometrical considerations (Figure 12), the surface concentrations are related to the volume fractions by

$$f_{LE^*} = h^* c_{LE^*}$$
$$c_{SiO_2} \cong 1 - c_{LE^*} \tag{16}$$

From this, the effective jump frequency can be approximated by

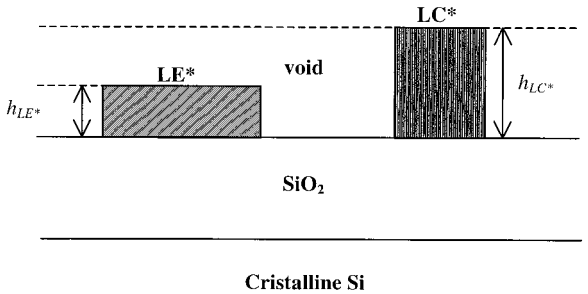

Figure 12. Simple geometrical model corresponding to the growth of an OTS monolayer on a SiO_2 surface. The native oxide can be either bare or covered by patches of OTS molecules in an expanded liquid (LE*) phase or in a condensed liquid (LC*) phase. The heights of the patches are, respectively, h_{LE^*} and h_{LC^*}.

$$\frac{1}{K_{eff}} \cong \frac{1}{K_{SiO_2}} - \frac{f_{OTS}}{h^*}\left(\frac{1}{K_{SiO_2}} - \frac{1}{K_{LE^*}}\right) \tag{17}$$

This equation has no parameter, and all the relevant quantities can be experimentally determined. This allows us to calculate an approximate value of K_{eff} and, by comparison with the directly measured values, to evaluate the range of validity of our initial hypothesis. It shows that the inverse of the effective jump frequency varies linearly with the volume fraction of the OTS (Figure 9, full line). For OTS volume fractions lower than 50%, the measured values and the approximated ones agree within the error bars. Under these conditions, the condensed liquid phase has almost no measurable effect on the wetting properties of the material either because its concentration is too low or because the corresponding jump frequency is too high. It should be pointed out that this upper limit seems to correspond to the complete coverage of the surface by molecules in the LE* phase, as previously described. In the later stages of the grafting process, the effect of the growing LC* phase cannot be neglected anymore.

For these stages, the LE* and LC* phases cover the whole surface and it is reasonable to assume that the surface fraction of the bare silica is negligible, although the void fraction measured by ellipsometry is not. Under these conditions,

$$\frac{1}{K_{eff}} \cong \frac{c_{LC^*}}{K_{LC^*}} + \frac{c_{LE^*}}{K_{LE^*}} \tag{18}$$

The OTS volume fraction is $f_{OTS} = f_{LE^*} + f_{LC^*}$ and can be expressed as

$$f_{OTS} = c_{LC^*} + h^* c_{LE^*} \tag{19}$$

This relation can be inverted and inserted in eq 18 to express K_{eff} as a function of f_{OTS}, the OTS volume fraction measured by ellipsometry and of the surface concentration of the expended liquid phase c_{LE^*}:

$$\frac{1}{K_{eff}} \cong \frac{f_{OTS}}{K_{LC^*}} + c_{LE^*}\left(\frac{1}{K_{LE^*}} - \frac{h^*}{K_{LC^*}}\right) \tag{20}$$

In contrast to eq 17, eq 20 is not an equation free of parameters. We therefore used it to calculate the c_{LE^*} values from the experimental values of $K^0_{,Weff}$. Once the c_{LE^*} values are known, the values of c_{LC^*} are calculated from eq 19 and the values of c_{SiO_2} from $c_{SiO_2} = 1 - (c_{LE^*} + c_{LC^*})$. During the early stages of the grafting process, the surface composition can be calculated from eq 16.

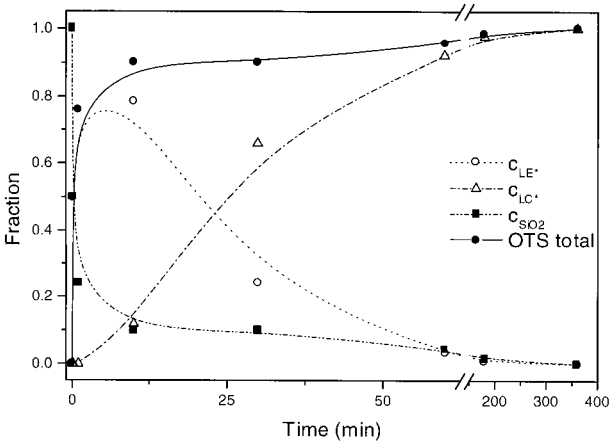

Figure 13. Time evolution of the different surface concentrations during the grafting process. During the early stages of the grafting process, the surface composition is calculated from eq 15. During the later stages, c_{LE^*} values are calculated from eq 19, the values of c_{LC^*} being obtained from eq 18 and the values of c_{SiO_2} from $c_{SiO_2} = 1 - (c_{LE^*} + c_{LC^*})$.

The surface composition, as well as the total OTS fraction, is represented in Figure 13. The SiO_2 surface fraction goes rapidly from 1.0 to 0.1 during the first minutes of the grafting process while the time evolution of the LE* phase exhibits a bell-shaped curve, reaching its maximum value after about 10 min to slowly decrease to zero afterward. This decrease clearly occurs in parallel with the onset of the LC* phase. The total OTS surface fraction already reaches 0.9 after 10 min. These results are in agreement with the AFM observations of Davidovits and co-workers,[21] although some differences could be noticed in terms of the time scale of the process.

4. Conclusions

In this study, we have determined the wetting properties of partially OTS-grated silicon wafers. The coverage of the surface was unambiguously characterized by the OTS volume fraction f_{OTS} measured using spectroscopic ellipsometry and effective media approximation. Time relaxation experiments of the contact angle of squalane droplets were also performed. The equilibrium contact angles appeared to follow a Cassie-like law. The relaxation data were processed using the molecular kinetic theory to evaluate the effective jump frequencies K_{eff} of the liquid molecules on the substrates as a function of the OTS volume fraction. K_{eff} remains more or less constant for f_{OTS} lower than 0.5 (i.e., during the onset of the expanded liquid phase) and sharply increases as a consequence of the transition from the expanded to the condensed liquid phase. It should be pointed out that the K_{eff} value are, during the onset of the condensed liquid phase, highly sensitive to the coverage of the substrate. That this approach may be generalized to other systems remains, however, an interesting open question. Furthermore, a simple geometrical model has been proposed to determine from the K_{eff} values the surface composition in two cases, the early and late stages of the grafting process, yielding results in agreement with AFM observations of similar systems.

Acknowledgment. This research has been partially supported by the Ministère de la Région Wallonne.

References and Notes

(1) Voinov, O. V. *Fluid Dyn.* **1976**, *11*, 714.
(2) Tanner, L. H. *J. Phys. D: Appl. Phys.* **1979**, *12*, 1473.
(3) Cox, R. G. *J. Fluid Mech.* **1986**, *168*, 169.
(4) Blake, T. D.; Haynes, J. M. *J. Colloid Interface Sci.* **1969**, *30*, 421.
(5) Drelich, J. *Colloid Surf. A* **1994**, *93*, 1.
(6) Andrieu, C.; Sykes, C.; Brochard, F. *Langmuir* **1994**, *10* (7), 2077.
(7) Drelich, J.; Wilbur, J. L.; Whitesides, G. M. *Langmuir* **1996**, *12* (7), 1913.
(8) Wiegand, G.; Jaworek, T.; Sackmann, E. *J. Colloid Interface Sci.* **1993**, *196* (2), 299.
(9) Topolski, K.; Urban, D.; Brandon, S.; De Coninck, J. *Phys. Rev. E*. **1997**, *56*, 3353.
(10) Urban, D.; Topolski, K.; De Coninck, J. *Phys. Rev. Lett.* **1996**,*76*, 4388.
(11) Collet, P.; De Coninck, J.; Dunlop, F.; Reignard, A. *Phys. Rev. Lett.* **1997**, *79*, 3704.
(12) Adão, M. H.; de Ruijter, M. J.; Voué, M.; De Coninck, J. *Phys. Rev. E* **1999**, *59*, 746
(13) Cassie, A. B. D. *Discuss. Faraday. Soc.* **1952**, *57*, 5041.
(14) de Ruijter, M. J.; De Coninck, J.; Blake, T. D.; Clarke, A.; Rankin, A. *Langmuir* **1997**, *13*, 7293.
(15) Blake, T. D.; Clarke, A.; De Coninck, J.; de Ruijter, M. J. *Langmuir* **1997**, *13*, 2164.
(16) Ulman, A. *An introduction to ultrathin organic films*; Academic Press: New York, 1991
(17) Silberzan, P.; Léger, L. *Phys. Rev. Lett.*, **1991**, *66*, 185.
(18) Roberts, G. G.; Pande, K. P.; Balrlow, W. A. *Proc. IEEE I* **1978**, *2*, 169.
(19) Boulas, C.; Davidovits, J.; Rondelez, F.; Vuillaume, D. *Microelectron. Eng.* **1995**, *28*, 217.
(20) Prime, K. L.; Whitesides, G. M. *Science* **1991**, *252*, 1164.
(21) Davidovits, J. V.; Silberzan, P.; Goldman, M. *J. Phys. Chem.*, submitted.
(22) Broszka, J. B.; Shahidzadeh, N.; Rondelez, F. *Nature* **1992**, *360*, 719.
(23) Schwatrz, D. K.; Steinberg, S.; Israelachvili, J.; Zasadzinski, J. A. N. *Phys. Rev. Lett.* **1992**, *69*, 3354.
(24) Britt, D. W.; Hlady, V. *J. Colloid Interface Sci.* **1996**, *178*, 775.
(25) Azzam, R. M. A.; Bashara, N. M. *Ellipsometry and polarized light*; North-Holland: Amsterdam, 1977.
(26) Tompkins, H. G. *A user's guide to ellipsometry*; Academic Press: New York, 1993.
(27) Aspnes, D. E.; Theeten, J. B.; Hottier, F. *Phys. Rev. B* **1979**, *20* (4), 3292.
(28) Bernoux, F.; Piel, J. P.; Lecat, J. H.; Stehlé, J. L. *Tech. Ing.'* **1990**, R6490-1−R6490-16.
(29) Bruggeman, D. A. G. *Ann. Phys. (Leipzig)* **1935**, *24*, 636.
(30) Voué, M. M. P.; Valignat, G.; Oshanin, A. M.; Cazabat; De Coninck, J. *Langmuir* **1998**, *14*, 5951.
(31) Rusanov, A. I.; Prokhorov, V. A. *Interfacial Tensiometry*; Elsevier: Amsterdam, 1996.
(32) de Ruijter, M. J. A microscopic approach of partial wetting: statics and dynamics. Ph.D. Thesis, Université de Mons-Hainaut, Mons, Belgium, 1998.
(33) Press, W. H.; Teukolsky, S. A.; Vetterling, W. T.; Flannery, B. P. *Numerical Recipes in Fortran*, 2nd ed.; Cambridge University Press: Cambridge, U.K., 1992.